MAGNETOHYDRODYNAMICS Vol. 60 (2024), No. 1–2, pp. 101–120
DOI: 10.22364/mhd.60.1–2.7

TWO GEOMETRIES FOR ALTERNATE LIQUID METAL MHD DISK GENERATOR

A. Alemany[1], *A. Montisci*[2], *A. Brekis*[3]

[1] *Grenoble Institute of Technology, INP, Simap Laboratory, Grenoble, France*
[2] *University of Cagliari, Italy*
[3] *Institute of Physics, University of Latvia, Latvia*
e-Mail: arturs.brekis@lu.lv

A quasi-static electric generator is presented and discussed. The quasi-static nature means that no solid moving part is envisaged, and the operating fluid remains contained within the device. More precisely, the generator is a liquid-metal MHD device activated by a pressure vibration that causes the liquid metal to oscillate in a DC magnetic field, giving rise to an electromotive force. Due to the high conductivity of the liquid metal, the induced electromotive force causes an alternating current circulating in the liquid metal. The liquid metal performs as a primary winding of a transformer, which is coupled with a secondary coil, wrapped in a way that it is co-axial with the liquid metal flow and connected to the electrical load. Alternate pressure can be provided by a wide range of processes, opening the possibility of using the proposed generator for harvesting energy from several renewable primary sources.

Introduction.

The need to implement energy transition poses a series of challenges to develop social, economic, and technological tools that make the use of renewable sources viable. One of the major obstacles is the high costs and low efficiency of energy harvesting systems, especially those that power domestic users. For example, the use of the main renewable sources, i.e. the sun and the wind, are both challenged due to the purchase cost and the impact on the environment throughout the entire life cycle. To give greater impetus to the transition process, it is necessary to develop high-efficiency and low-cost technologies. The present study fits into this trend, as it consists of a highly efficient and available electromechanical conversion system that can be coupled with most renewable sources. In [1], authors describe how the main renewable sources, such as solar radiation, biomass, wind, rivers, and sea waves, are susceptible to being converted into vibration power. Therefore, the device proposed in this paper is intended to be integrated into a hybrid renewable energy system.

In particular, in the present study, the design parameters of the device are thought to be embedded in a thermoacoustic-MHD generation system supplied by solar radiation. Thermoacoustics [2] is a quasi-static thermodynamic process allowing the conversion of heat into mechanical energy in the form of a pressure wave. The phenomenon is triggered when the gradient of temperature overcomes a critical value, and its efficiency of conversion depends on such gradient, i.e. the greater the gradient, the higher the efficiency. By coupling the thermoacoustic generator with an electrical generator, electrical energy in an AC form is produced. The two-stage thermoelectric conversion is compatible with a large variety of heat sources at different levels of temperatures, such as solar radiation, combustion, and exhaust heat of industrial processes. Of great interest among them is the sun as a freely available source throughout the world. Furthermore, due to the possibility of radiation concentration, very high temperatures can be reached, and as a consequence, the reference Carnot efficiency could reach very high values.

Liquid metal MHD (LMMHD) generators [3], [4], [5], especially disk ones, represented a possible alternative when, at the end of the last century it was realized that the open-cycle MHD generation posed technological issues difficult to overcome. Those were essentially the need for a high conductive plasma [6], intense magnetic fields [7], corrosion-resistant electrodes [8]. The difficulty in realizing such properties of the operating fluid was determined by the fact that it was made up of combustion products, which themselves do not have very high conductivity [9]. It was, therefore, necessary to seed the gas using metals [10], which, however, were difficult to recover at the end of the cycle. Liquid metals have the advantage of having a conductivity of several orders of magnitude higher than combustion gases, so there is no need for seeding, and the applied magnetic field can be much less intense since the induction effect occurs at weakly induced tensions. The problem of corrosion is also mitigated because the generator can operate at low temperatures, so one of the main factors, although not the only one responsible for the deterioration of electrodes, is eliminated. On the other hand, the liquid metal changes its volume negligibly as the temperature increases, so it alone is not suitable for converting thermal energy into electrical. This limit has been overcome in [11], [12], where a two-stage conversion system is envisaged, the first stage of which transforms heat into mechanical vibration energy, whereas the other includes a liquid metal MHD generator which transforms the energy of vibration into electrical energy. Since the input power to the MHD generator is alternate, the transfer of power to the load occurs through a magnetic coupling. Therefore, the problem of electrodes, which are no longer foreseen, is definitively solved.

This makes it possible to achieve a global chain efficiency of 50%, which is out-of-reach for a photovoltaic panel. Indeed, the proposed system takes advantage of the fact that the entire solar spectrum contributes to increasing the temperature of the solar collector, whereas only a limited band is exploited by the photovoltaic cell to produce electricity, and most of the radiation has the only effect of increasing the operating temperature, decreasing so the efficiency.

The present study adds to the work presented in [13], where an identical layout is described by neglecting viscosity. The viscous losses there are considered in the Navier–Stokes equation, and then the assumption of a uniform distribution of velocity in the cross-section of the channel is replaced by a more realistic distribution of velocity, considering the boundary layer at the wall.

In [14], a system implementing the same functioning principle was developed and tested experimentally in the framework of the EU-funded project called SpaceTRIPS [15]. The geometry of the generator presented in this paper differs from the prototype developed in SpaceTRIPS because instead of two free surfaces where the supply pressure is applied to, in the present case, the supply pressure is applied to one side, and the other end of the supply pressure is substituted by a resonant cavity.

The generator developed in the SpaceTRIPS project was aimed at generating electricity in space using isotopes (Americium, Plutonium) as a heat source of the thermoacoustic engine and a radiative cooler as a cold sink [4], [3]. The main advantage in the space domain arises from the static nature of such a device, which allows to tackle critical aspects of space missions, such as inertia forces and the robustness of equipment during take-off operations.

The layout described in the present paper is focused on earth applications, where gravity plays a significant role, and for this reason, the vertical position is considered. In the future, the goal is to develop a hybrid energy system that is able to supply a house or

a group of houses by different renewable primary sources, all using the presented device to convert vibration energy into electrical energy. The target is determined by the specific nature of the single primary source.

The paper is organized as follows. In Section 1, the geometry of the generator is described. In Section 2, the main assumptions and the design parameters are given. In Section 3, the equations of the model are derived. In Sections 4 and 5, the equations are solved. In Sections 6, 7, and 8, the results are given and commented on. Section 9 presents conclusions.

1. Description of two geometries under study.

The principle of the process is presented in Fig. 1. A liquid metal is contained in an axisymmetric vessel made of ferromagnetic material. The vessel is hollow inside, with a central duct that communicates with a toroidal cavity by means of a disk channel. The central duct and the channel are completely filled with liquid metal, whereas the cavity is partially filled with gas. The channel is magnetized by a permanent magnet placed on the bottom, which generates a vertical DC magnetic field. The ferromagnetic vessel is shaped to create an electromagnet, where the channel represents a gap. Finally, a coaxial coil with the ferromagnetic vessel is placed to be magnetically coupled with the channel. Two different layouts are considered for the coil, respectively, vertical, and planar.

Oscillating pressure is applied to the free surface of the liquid metal on the top of the central duct. The pressure vibration induces a radial alternate motion of the liquid in the channel, crossing the DC magnetic field generated by the permanent magnet. The interaction between the liquid metal and the magnetic field induces an electromotive force in the liquid metal, causing the circulation of a longitudinal alternating current. Such current performs as the primary winding of the transformer, where the coil represents the secondary winding which is electrically connected to the load. Provided that the entire process is maintained within the range of linearity, the voltage which supplies the load has the same frequency as the applied pressure.

To make it possible to apply alternate pressure, counter pressure is applied by means of the cavity filled with a gas that reacts to the liquid oscillations with a phase shift depending on the characteristic of the system. The nature of the gas and the average pressure strongly affect the device performance. The average pressure must be higher than the amplitude of the oscillating component, but it is preferable to keep a margin with respect to this limit. In this study, it was assumed that the amplitude of the oscillation was less than 10% of the average pressure (20–50 bar).

2. Main hypothesis and parameters.

The height profile of the channel is shaped in order to keep the cross-section constant along the radius, and as a consequence, the velocity in the channel is also constant:

$$e(r) = e_0 \frac{r_0}{r}, \tag{2.1}$$

where r is the radial coordinate, $e(r)$ is the height profile of the channel along the radius, r_0 is the radial coordinate of the channel inlet, and e_0 is the corresponding height of the channel. So it is clear from Eq. (1) that the total cross-section concerning the flow rate of the liquid metal, which is $2\pi r e(r) = \text{const} = 2\pi r_0 e_0$, is constant, and, hence, at a given time, the velocity is constant, neglecting the very small boundary layer (see explanation).

The vertical induction field applied by the permanent magnet due to the height reduction of the channel increases in intensity along the radial direction approximately

as

$$B(r) = B_0 \frac{r}{r_0} \tag{2.2}$$

where $B(r)$ is the intensity of the applied induction along the radius, B_0 is the intensity at the inlet of the channel. Assuming this profile implies that both the end effects and the curvature of the streamlines of induction are neglected. This is possible if the height of the channel is small, which is the considered situation.

Referring to Figs. 1*a*,*b*,*c*, the ferromagnetic material is supposed to have infinite permeability, whereas the conducting liquid in the channel is assumed to have the magnetic permeability of vacuum.

The coil (horizontal or vertical) inside the ferromagnetic material is subjected to the induced magnetic field oscillation, which results in the AC-induced current inside the liquid metal. The corresponding induced voltage depends on the number of turns N of the coil and on the coil configuration. In the vertical configuration (Fig. 1*a*), each turn of the coil is subjected to the induced magnetic flux so that the total flux is the product of the flux in one turn multiplied by the number of turns N.

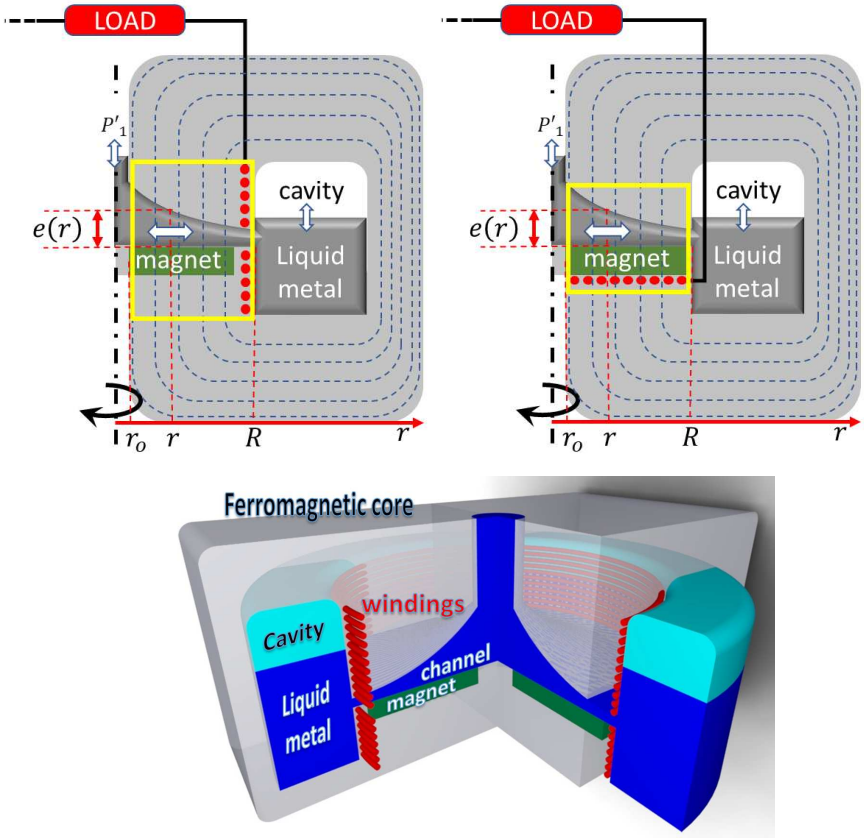

Fig. 1. The principle of the process: (*a*) disk generator with a vertical coil, (*b*) disk generator with a horizontal coil, (*c*): complete view of the disk generator with the vertical coil (*a*). The geometry is almost the same as in (*b*).

In the horizontal configuration, each turn is related to a part of the total flux which depends on its radial position so that at a radial distance r from the center of the generator the number of turns N related to the magnetic flux is

$$n = N\frac{r - r_0}{R - r_0} \tag{2.3}$$

Considering the influence of viscosity, as said above, the velocity is assumed to be almost constant along the disk channel. However, due to the viscosity, a boundary layer is formed in the proximity of the wall of the channel. The depth δ_ν of the boundary layer is controlled by the frequency according to

$$\frac{\delta_\nu}{r_0} = \sqrt{\frac{1}{R_\omega}}, \quad \text{with} \quad R_\omega = \frac{\omega {r_0}^2}{\nu}. \tag{2.4}$$

In this expression, R_ω is the Reynolds number, and ν is the kinematic viscosity. In the following, it is assumed that δ_ν is very small, such as

$$\frac{\delta_\nu}{r_0} \ll 1 \rightarrow R_\omega \gg 1. \tag{2.5}$$

This condition is perfectly verified even for a very small value of ω. Considering Eq. (2.5) and taking into account the geometry and values given in Table 1 yield $\omega \gg 10^{-2}/16$. In the present study, the value of ω, i.e. the oscillating value of pressure and velocity, is of the order $\omega \sim 314$, corresponding to the 50 Hz frequency.

Under this condition, the boundary layer is confined at a very small depth near the wall, so it is assumed that the core flow at a constant velocity occupies almost the full section. However, the viscous dissipation decreases efficiency.

As to the pressure, the use of thermoacoustics to produce mechanical energy is necessary to consider the known fact that the higher the average pressure, the greater the efficiency. Therefore, to obtain good efficiency, it is necessary to impose a sufficiently high pressure. The oscillating pressure strictly depends on this imposed value since a suitable value for its amplitude must be within 5–10% of the average value.

3. Analytical model.

The analytical model is presented by the Navier–Stokes equation and the induction equation. In cylindrical coordinates, assuming the symmetry conditions so that $\partial/\partial\theta = 0$ and, due to the small value of the channel depth $\partial/\partial z = 0$, the two equations are written, respectively, as

$$\frac{\partial V}{\partial t} + V\frac{\partial V}{\partial r} = -\frac{1}{\rho}\frac{\partial p}{\partial r} + \nu\left(\frac{1}{r}\frac{\partial r}{\partial}\frac{\partial V}{\partial r} + \frac{\partial^2 V}{\partial z^2} - r^2\right) - \frac{B}{\mu_0}\frac{\partial b}{\partial r}, \tag{3.1}$$

$$\frac{\partial b}{\partial t} = -\frac{1}{r}\frac{\partial}{\partial r}r\,(BV) + \frac{1}{\mu\sigma}\left(\frac{\partial^2 b}{\partial z^2} + \frac{\partial^2 b}{\partial r^2} + \frac{1}{r}\frac{\partial b}{\partial r}\right). \tag{3.2}$$

On the other hand, it is supposed that the induced field b is much smaller than the applied one B_0:

$$\frac{b}{B} \ll 1. \tag{3.3}$$

The conditions for which this hypothesis is satisfied will be given below. It is assumed that the total penetration of the pulsating magnetic field into the domain is given by

$$\frac{\delta_{\mathrm{m}}}{e(r)} \sim \sqrt{\frac{1}{\sigma\mu\omega e^2(r)}} \gg 1 \to \sigma\mu\omega e^2(r) \ll 1 \to \sigma\mu\omega {e_0}^2 \ll 1, \tag{3.4}$$

with δ_{m} being the depth of penetration of the induced magnetic field, σ the conductivity of the liquid metal, ω the angular frequency. Under these operative conditions, the Prandtl number is very high:

$$\mathrm{Pr} = \nu\mu\sigma \gg 1. \tag{3.5}$$

The magnetic field penetration in the gap is assumed, Eq. (3.4), and then the term

$$\frac{\partial^2 b}{\partial z^2} \sim \frac{\Delta b}{\delta_{\mathrm{m}}^2}$$

must be lower than the term concerning the derivation against

$$r\frac{\partial^2 b}{\partial r^2} \sim \frac{b}{R^2}$$

so that

$$\frac{\Delta b}{\delta_{\mathrm{m}}^2} \ll \frac{b}{R^2} \to \frac{\Delta b}{b} \ll \frac{\delta_{\mathrm{m}}^2}{R^2} \to \mu\sigma\omega R^2 \gg 1, \tag{3.6}$$

where R is the external radius of the channel. So, assuming that the cross-section of the channel is such that the velocity is quasi-constant at a given time for any value of the radial position, the continuity equation for mass conservation is identically satisfied.

To conclude, the range of values, where the proposed solution is available, is $R_\omega \gg 1$ and $\mu\sigma\omega R^2 \gg 1$. Both conditions are satisfied when $\omega \gg 1/(\mu\sigma R^2) \approx 3$ in terms of Table 1. These small values are compatible with any oscillating source of energy.

The governing equations read as

$$\frac{\partial V}{\partial t} = -\frac{1}{\rho}\frac{\partial p}{\partial r} + \nu\left(\frac{1}{r}\frac{\partial}{\partial r}r\frac{\partial V}{\partial r} + \frac{\partial^2 V}{\partial z^2} - \frac{V}{r^2}\right) - \frac{B_0}{\mu_0}\frac{\partial b}{\partial r}, \tag{3.7}$$

$$\frac{\partial b}{\partial t} = -\frac{1}{r}\frac{\partial}{\partial r}\left(rVB_0\right) + \frac{1}{\mu\sigma}\frac{1}{r}\frac{\partial}{\partial r}\left(r\frac{\partial b}{\partial r}\right). \tag{3.8}$$

4. General solution.

4.1. Velocity. Under the hypothesis of a small value of the channel height, the derivative of Eq. (3.8) gives:

$$\frac{\partial^2 b}{\partial z \partial t} \sim 0 \to \frac{\partial}{\partial z}\left[\frac{1}{r}\frac{\partial}{\partial r}\left(rVB_0\right) + \frac{1}{\mu\sigma}\frac{1}{r}\frac{\partial}{\partial r}\left(r\frac{\partial b}{\partial r}\right)\right] = 0 \to \frac{1}{r}\frac{\partial}{\partial r}\left(r\frac{\partial V}{\partial z}B_0\right) = 0, \tag{4.1}$$

from which we derive

$$r\frac{\partial V}{\partial z}B_0 = \Phi(z) \to \frac{\partial V}{\partial z} = \frac{\Phi(z)}{B_0 r}. \tag{4.2}$$

It is assumed that the velocity oscillations have the same frequency as the applied pressure, and the pressure gradient in the z-direction can be neglected due to the small

depth of the channel. By deriving the velocity equation in the z-direction, and re-writing the equation in phasorial terms we have

$$i\omega\frac{\partial V}{\partial z}=\nu\left(\frac{1}{r}\frac{\partial}{\partial r}r\frac{\partial}{\partial r}\frac{\partial V}{\partial z}-\frac{1}{r^2}\frac{\partial V}{\partial z}+\frac{\partial^3 V}{\partial z^3}\right). \tag{4.3}$$

By introducing the expression of velocity into the function $\Phi(z)$, after some algebraic steps, the above expression reads:

$$\Phi(z)\left(i\omega+\frac{\nu}{r^2}-\frac{4\nu}{r^2}\right)=\nu\frac{\partial}{\partial z^2}\Phi(z). \tag{4.4}$$

According to the hypothesis of $R_\omega \gg 1$ (Eq. 2.5), the influence of viscosity is limited to a small distance from the wall. Therefore, the velocity distribution will be considered to be organized in the core and boundary layers. In the core, the velocity is assumed to be constant. Consequently, the velocity profile in the cross-section of the channel will be described only in the boundary layer. Let ξ be the distance from the wall,

$$\xi=\frac{e(r)}{2}-z\rightarrow z=\frac{e(r)}{2}-\xi,\quad \frac{\mathrm{d}}{\mathrm{d}z}=-\frac{d}{d\xi}, \tag{4.5}$$

and then the governing equation for the velocity becomes

$$\Phi(\xi)\left(i\omega-\frac{3\nu}{r^2}\right)-\nu\frac{\mathrm{d}\Phi(\xi)}{\mathrm{d}\xi^2}=0. \tag{4.6}$$

The general solution assumes that $R_\omega \gg 1$ such as $\omega/\nu \gg 3/r^2$ is of the form

$$\Phi(\xi)=C_1(r)\mathrm{e}^{\sqrt{i\omega/\nu}\xi}+C_2(r)\mathrm{e}^{-\sqrt{i\omega/\nu}\xi}. \tag{4.7}$$

Considering the boundary conditions,

$$(\xi\rightarrow\infty)\Rightarrow\left(\frac{\partial V(\xi)}{\partial\xi}\rightarrow 0\right),\quad (\Phi(\xi)\rightarrow 0)\Rightarrow C1=0, \tag{4.8}$$

and

$$\xi=0\Rightarrow V=0. \tag{4.9}$$

Finally, by considering the incompressibility of the fluid and that the flow rate Q_0 is such that $V_0=Q_0/(2\pi e_0 r_0)$ it yields:

$$V=V_0\left(1-\mathrm{e}^{-\sqrt{i\omega/\nu}\,\xi}\right)=V_0\left(1-\mathrm{e}^{-\sqrt{i\omega r_0^2/\nu}\,\xi r_0^{-1}}\right)=V_0\left(1-\mathrm{e}^{-\sqrt{i\omega R_\omega}\,\xi r_0^{-1}}\right). \tag{4.10}$$

As seen above, when $R_\omega \gg 1$, the depth of the boundary layer is extremely small so that the deficit of the flow rate due to the viscosity action can be neglected, and then, for an incompressible fluid, the velocity inside the channel corresponding to Eq. (4.10) does not vary in the r-direction.

The evolution of velocity over time is

$$V=V_0\left[\mathrm{e}^{i\omega t}-\frac{\mathrm{e}^{i\left(\omega t-\sqrt{\omega/(2\nu)}\,\xi\right)}}{\mathrm{e}^{\sqrt{\omega/(2\nu)}\,\xi}}\right]. \tag{4.11}$$

This evolution characterizes a damped wave with the evolution at the celerity

$$c = \frac{\omega}{\sqrt{2\omega/\nu}/2} = \sqrt{2\omega\nu} \tag{4.12}$$

with the wavelength

$$\lambda = \frac{4\pi}{\sqrt{2}}\sqrt{\frac{\nu}{\omega}} \tag{4.13}$$

and the depth of penetration

$$\delta \sim \frac{1}{\sqrt{\omega/(2\nu)}} = \sqrt{2\frac{\nu}{\omega}} \Rightarrow \frac{\delta}{r_0} = \sqrt{2\frac{\nu}{r_0^2\omega}} \ll 1 \Rightarrow \frac{r_0^2\omega}{\nu} = R_\omega \gg 1. \tag{4.14}$$

This condition is well satisfied in the present situation and geometry.

It is worth recalling briefly what velocity conditions have been obtained in [13]. It is assumed that viscosity is active only in a very small layer near the wall at $R_\omega \gg 1$ when, on the contrary, the induced magnetic field indicates a full penetration into the channel, so $\mu\sigma\omega R^2 \gg 1$. This is mainly the effect of the Prandtl number, $\mathrm{Pr} = \nu\mu\sigma \gg 1$.

Even if the boundary layer is small, this does not mean that the action of viscosity can be neglected, and the corresponding energy dissipation due to its action will be given further.

4.2. Induced magnetic field. It is assumed that the induced magnetic field has a constant value across the depth of the channel and that the fluid velocity is only slightly affected by the viscosity, $R_\omega > 1$. Consequently, the core of the flow with velocity $V = V_0 \mathrm{e}^{i\omega t}$ is taken as the origin of the phase when the solution is calculated in a complex form.

The induced magnetic field is governed by Eq. (3.8). Due to the assumptions for the applied magnetic field all along the channel Eq. (2.2) and the profile of the channel Eq. (2.1), which yields a constant cross-section, the source term of the induced field $-1/r\partial/\partial r[rV_0I(r)]$ is constant in the radial direction:

$$c = -2V_0B_0/r_0, \tag{4.15}$$

with B_0 being value of the applied field for $r = r_0$. Let the following dimensionless variables be

$$r' = \frac{r}{r_0}, \quad b'(r) = \frac{b(r)}{B_0}. \tag{4.16}$$

The dimensionless governing equation of the induced magnetic field reads

$$i\frac{\mathrm{Rm}\omega r_0}{V_0}b' = -2\mathrm{Rm} + \frac{1}{r'}\frac{\partial}{\partial r'}\left(r'\frac{\partial b'}{\partial r'}\right), \tag{4.17}$$

where $\mathrm{Rm} = V_0r_0\mu\sigma$ is the magnetic Reynolds number, μ is the magnetic permeability of the conducting fluid assumed to have the value of vacuum, and σ is its electrical conductivity. Eq. (4.17) is a second-order differential equation with variable coefficients that does not present a solution in a closed form. By removing the primes in the variables, the induced magnetic field equation admits a solution in the form

$$b(r) = \gamma_1 I_0(X) + \gamma_2 K_0(X) + \frac{2iV_0}{\omega r_0} = \gamma_1 I_0(X) + \gamma_2 K_0(X) + \frac{2i\mathrm{Rm}}{\mathrm{Rm}^*}, \tag{4.18}$$

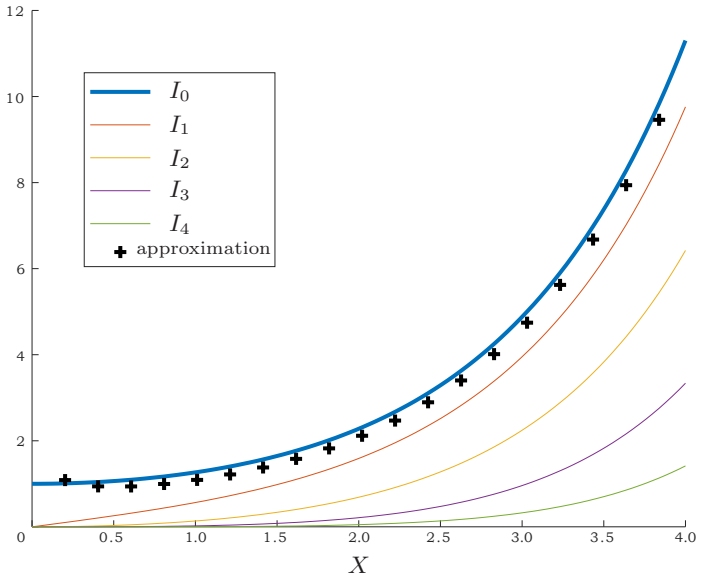

Fig. 2. Comparison between I_0 and the derived expression (16?) for real X.

where $X = \sqrt{i\mathrm{Rm}^*}\, r/r_0$, $I_0(X)$, and $K_0(X)$ are the modified Bessel's functions of zero order, and $\mathrm{Rm}^* = r_0^2 \omega\mu\sigma$ which has the same form as the magnetic Reynolds number and characterizes the skin effect. For symmetry reasons, the constant γ_2 is null, and the solution is as

$$b(r) = \gamma_1 I_0(X) + \frac{2iV_0}{\omega r_0} = \gamma_1 I_0(X) + \frac{2iRm}{\mathrm{Rm}^*}. \tag{4.19}$$

The expression for γ_1 depends on the boundary conditions. To determine this coefficient in the following, the Ampère theorem and Faraday law will be used. Furthermore, to simplify the calculations, an approximated expression of the Bessel function of zero order has been used [3]:

$$I_0(X) \cong \frac{1}{\sqrt{2\pi X}} \mathrm{e}^X = \frac{1}{\sqrt{2\pi\sqrt{i\mathrm{Rm}^*}\, r/r_0}} \mathrm{e}^{\sqrt{i\mathrm{Rm}^*} r/r_0} \tag{4.20}$$

with a very good precision compared with the true values when X is higher than 0.5 (Fig. 2).

5. Integration constant for each considered geometry.

The characteristics of the electrical generator depend on the constant γ_1 that arises from the geometry of the engine and arrangement of the coil. In the previous study, the coil was assumed to be perpendicular to the channel [1], and viscosity was neglected. This study considers two geometries of the coil and viscosity in the realistic hypothesis of $r_0^2\omega/\nu = R_\omega \gg 1$ (Eq. 4.11). The constant γ_1 is calculated using two equations, the first one being the Ampère's theorem and the second one from the coil electrical circuit.

5.1. Ampère's theorem.

Applied to yellow contour in Figs. 1*a*,*b*, it gives

$$b(r_0)e_0 = \mu NI - \int_{r_0}^{R} \frac{\mathrm{d}b}{\mathrm{d}r} e(r)\mathrm{d}r, \tag{5.1}$$

where N is the total number of turns in the coil, I is the electric current supplying the electrical load, and the last term is the induced current in the conducting fluid. Introducing expression (4.19) into (5.1), the following first equation is derived:

$$\gamma_1 B_0 \left\{ e_0 \int_1^{R/r_0} \frac{\mathrm{d}I_0\left(X\right)}{\mathrm{d}r} \frac{1}{r}\mathrm{d}r + \left(I_0\left(X_I\right) + \frac{2i\mathrm{Rm}}{\gamma_1 \mathrm{Rm}^*} \right) e_0 \right\} = \mu NI, \tag{5.2}$$

where e_0 is the value of $e(r)$ for $r = r_0$.

5.2. Equation for the coil electric circuit.

To complete the boundary conditions, the Maxwell–Ampere equation together with the Ohm's law is used:

$$-i\omega\Phi = RI \tag{5.3}$$

with Φ being the magnetic flux through the coil which has N turns, and R the load resistance. This gives from Eq. (5.3) for the vertical coil

$$N \left[-\gamma_1 \frac{i\omega B_0 \sqrt{2\pi} r_0^2 \mathrm{e}^{-i\pi/8}}{\mathrm{Rm}^*} \int_{\sqrt{\mathrm{Rm}^*}}^{\sqrt{\mathrm{Rm}^*} R r_0^{-1}} \sqrt{\rho} \mathrm{e}^{\rho \mathrm{e}^{i\pi/4}} \mathrm{d}\rho + 2\pi r_0 u_0 B_0 \left(\frac{R^2}{r_0^2} - 1 \right) \right] = RI, \tag{5.4}$$

and for the horizontal coil

$$\begin{aligned} -i\omega B_0 N r_0^2 \Bigg\{ & \frac{\gamma_1}{R - r_0} \frac{\sqrt{2\pi}}{\mathrm{Rm}^*} \int_{r_0}^{R} \int_{\sqrt{\mathrm{Rm}^*}}^{\sqrt{\mathrm{Rm}^*} R r_0^{-1}} \frac{\mathrm{e}^{-i\pi/8} \mathrm{e}^{\rho \mathrm{e}^{i\pi/4}}}{\sqrt{\rho}} \mathrm{d}r + \\ & \frac{i2\pi}{R/r_0 - 1} \frac{\mathrm{Rm}}{\mathrm{Rm}^*} \left[\frac{(R/r_0)^3 - 1}{3} - \left(\frac{R}{r_0} - 1 \right) \right] \Bigg\} = RI, \end{aligned} \tag{5.5}$$

where the expression for I_0 has been approximated according to (4.20), and $\rho = \sqrt{\mathrm{Rm}^*} r / r_0$ is a dimensionless variable. The combination of Eqs. (5.3) and (5.4) for the vertical coil and (5.3) and (5.5) for the horizontal one allows to find γ_1 for both geometries.

For the vertical coil,

$$\begin{aligned} \gamma_1 = & \left\{ \frac{2\pi \mathrm{e}^{i\pi/8} \mathrm{Rm} N^2}{\sigma e_0 R I} \left[-\frac{i\sigma e_0 R}{\pi N^2 \mathrm{Rm}^*} + \left(\frac{R^2}{r_0^2} - 1 \right) \right] \right\} \\ & \left\{ \left[\frac{\mathrm{e}^{\sqrt{\mathrm{Rm}^*} \mathrm{e}^{i\pi/4}}}{\sqrt{2\pi\sqrt{\mathrm{Rm}^*}}} + \sqrt{\mathrm{Rm}^*} \int_{\sqrt{\mathrm{Rm}^*}}^{\sqrt{\mathrm{Rm}^*} R r_0^{-1}} \frac{1}{\rho} \frac{\mathrm{d}}{\mathrm{d}\rho} \left(\frac{1}{\sqrt{2\pi\rho}} \mathrm{e}^{\rho \mathrm{e}^{i\pi/4}} \right) \mathrm{d}\rho \right] \right. \\ & \left. + iN^2 \frac{\sqrt{2\pi}}{\sigma e_0 R} \int_{\sqrt{\mathrm{Rm}^*}}^{\sqrt{\mathrm{Rm}^*} R r_0^{-1}} \sqrt{\rho} \mathrm{e}^{\rho \mathrm{e}^{i\pi/4}} \mathrm{d}\rho \right\}^{-1} \end{aligned} \tag{5.6}$$

and for the horizontal coil,

$$\gamma_1 = \mathrm{e}^{i\frac{\pi}{8}} \frac{2\pi N^2 \mathrm{Rm}}{\sigma e_0 R} \left\{ -i \frac{\sigma e_0 R}{\pi N^2 \mathrm{Rm}^*} + \left[\frac{(R/r_0)^3 - 1}{3\,(R/r_0 - 1)} - 1 \right] \right\}$$
$$\left\{ \left[\frac{\mathrm{e}^{\sqrt{\mathrm{Rm}^*}\mathrm{e}^{i\pi/4}}}{\sqrt{2\pi\sqrt{\mathrm{Rm}^*}}} + \sqrt{\mathrm{Rm}^*} \int_{\sqrt{\mathrm{Rm}^*}}^{\sqrt{\mathrm{Rm}^*} R r_0^{-1}} \frac{1}{\rho} \frac{\mathrm{d}}{\mathrm{d}\rho} \left(\frac{1}{\sqrt{2\pi\rho}} \mathrm{e}^{\rho \mathrm{e}^{i\pi/4}} \right) \mathrm{d}\rho \right] \right. \tag{5.7}$$
$$\left. + iN^2 \frac{\sqrt{2\pi}}{e_0 \sigma r_0 R\,(R/r_0 - 1)} \int_{r_0}^{R} \int_{\sqrt{\mathrm{Rm}^*}}^{\sqrt{\mathrm{Rm}^*} r r_0^{-1}} \sqrt{\rho} \mathrm{e}^{\rho \mathrm{e}^{i\pi/4}} \mathrm{d}\rho \mathrm{d}r \right\}^{-1}$$

from which all other quantities can be expressed.

6. Pressure distribution along the channel.

The pressure applied at the free surface of the central duct of the generator controls the mechanical power supplied to the engine given by a scalar product between the applied pressure and the flow rate of the liquid metal.

The drag force is applied to the liquid by the pressure difference $p'_1 - p'_2$ between the two free surfaces. This pressure difference depends on several parameters, independently of the geometry of the engine, such as Joule losses and viscous losses.

There are two ways to estimate this pressure difference. The first one is to apply the Bernoulli theorem in its extended version, considering the non-stationary flow and the presence of electromagnetic and viscosity losses. Another solution will be used here which considers the kinetic energy theorem applied to the entire mass of liquid for a time interval δt:

$$W = \delta E_{\mathrm{K}} = \frac{1}{2} \int_{V_{M'}} \rho V_0^2(t + \mathrm{d}t)\mathrm{d}v - \frac{1}{2} \int_{V_{M'}} \rho V_0^2(t)\mathrm{d}v$$
$$= P'_1 U'_1 S'_1 \mathrm{d}t - P'_2 U'_2 S'_2 \mathrm{d}t + \left(\int_{V_{M'}} (\nabla \times \mathbf{b}) \times \mathbf{B_0} \mathrm{d}r \right) S V_0(t)\mathrm{d}t + W_\nu \mathrm{d}t, \tag{6.1}$$

where W is the work of external and internal forces, including Joule dissipation, and W_ν is the dissipation due to viscosity, δE_{K} is the variation of kinetic energy, $V_{M'}$ is the volume of liquid, U_1 is the velocity of the free surface in the central duct with the cross-section S_1 and subject to the pressure P_1; U_2 is the velocity of the free surface in the cavity with the cross-section S_2 and subject to the pressure P_2, and, finally, S is the cross-section of the channel.

By developing expression (6.1) in the three volumes of liquid, it writes:

$$\int_{V_1} \rho \left(V_1 \frac{\mathrm{d}V_1}{\mathrm{d}t} \right)_t \mathrm{d}t\mathrm{d}v + \int_{V} \rho \left(V \frac{\mathrm{d}V}{\mathrm{d}t} \right)_t \mathrm{d}t\mathrm{d}v + \int_{V_2} \rho \left(V_2 \frac{\mathrm{d}V_2}{\mathrm{d}t} \right)_t \mathrm{d}t\mathrm{d}v =$$
$$P'_1 V_1 \mathrm{d}t - P'_2 V_2 \mathrm{d}t + \left[\frac{1}{\mu} \int_V (\mathrm{rot}\mathbf{b} \wedge \mathbf{B})\,\mathrm{d}v \right] V \mathrm{d}t + W_\nu \mathrm{d}t. \tag{6.2}$$

The expression for the viscous losses W_ν will be given below. Considering that the velocity along the channel is constant at a given time and since the integral $\rho \mathrm{d}v$ over the volume is nothing but the mass of each of the three parts, we derive

$$\begin{aligned} M_1\left(V_1\frac{\mathrm{d}V_1}{\mathrm{d}t}\right)_t \mathrm{d}t + m\left(V\frac{\mathrm{d}V}{\mathrm{d}t}\right)_t \mathrm{d}t + M_2\left(V_2\frac{\mathrm{d}V_2}{\mathrm{d}t}\right)_t \mathrm{d}t = \\ P_1' V_1 S_1 \mathrm{d}t - P_2' V_2 S_2 \mathrm{d}t + \left[\frac{1}{\mu}\int\limits_V (\mathrm{rot}\mathbf{b}\wedge\mathbf{B})\,\mathrm{d}v\right]_t + SV\mathrm{d}t + W_\nu \mathrm{d}t, \end{aligned} \tag{6.3}$$

and finally,

$$\begin{aligned} M_1\left(V_1 i\omega V_1\right)_t \mathrm{d}t + m\left(V i\omega V\right)_t \mathrm{d}t + M_2\left(V_2 i\omega V_2\right)_t \mathrm{d}t = \\ P_1' V_1 S_1 \mathrm{d}t - P_2' V_2 S_2 \mathrm{d}t + \left[\frac{1}{\mu}\int\limits_V (\mathrm{rot}\mathbf{b}\wedge\mathbf{B})\,\mathrm{d}v\right]_t V\mathrm{d}t + W_\nu \mathrm{d}t, \end{aligned} \tag{6.4}$$

where M_1, m, and M_2 are, respectively, the mass of the liquid in the central column, in the disk channel and in the cavity. In Eq. (6.4), the first three terms represent the inertia forces, two terms on the right-hand side are the power of the pressure forces applied to the free surfaces of the central duct and cavity, and two last terms denote the power of the electromagnetic forces and the dissipation due to viscosity. After reduction, Eq. (6.3) writes

$$P_1' = P_2' + \frac{i\omega V_C M'}{s} + \frac{B_{\mathrm{ro}}^2 \gamma_1 \mathrm{e}^{-i\pi/8}}{\sqrt{2\pi}\mu\sqrt{\mathrm{Rm}_{\mathrm{m}}^*}} \int\limits_{\sqrt{\mathrm{Rm}^*}}^{\sqrt{\mathrm{Rm}^*}Rr_0^{-1}} \frac{\partial}{\partial\rho}\left(\frac{\mathrm{e}^{\rho \mathrm{e}^{i\pi/4}}}{\sqrt{\rho}}\right)\rho\mathrm{d}\rho + \frac{W_\nu}{V_0 S}. \tag{6.5}$$

The law of perfect gas was assumed for the cavity under the hypothesis of a small variation of the oscillating pressure:

$$\frac{P_2'}{P_0} \ll 1, \tag{6.6}$$

where P_0 is the mean pressure imposed in the system. After some simple first-order approximations and assuming adiabatic evolution, the following expression is derived:

$$P_2' = -i\frac{\gamma P_0 V_C s}{\omega V_{M'}}, \tag{6.7}$$

where $\gamma = C_{\mathrm{p}}/C_{\mathrm{v}}$ is the ratio of thermal capacities at constant pressure and volume. Finally,

$$\begin{aligned} P_1' = \frac{\mathrm{Rm}}{\mathrm{Rm}^*}\left(-i\frac{\gamma P_0 r_0 S}{V_C} + \frac{i\mathrm{Rm}^{*2} M'}{s(\mu\sigma)^2 r_0^3}\right) \\ + \frac{B_0^2}{\mu\sqrt{2\pi\mathrm{Rm}^*}}\mathrm{e}^{-i\pi/8}\gamma_1 \int\limits_{\sqrt{\mathrm{Rm}^*}}^{\sqrt{\mathrm{Rm}^*}Rr_0{}^{-1}} \frac{\partial}{\partial\rho}\left(\frac{\mathrm{e}^{\rho \mathrm{e}^{i\pi/4}}}{\sqrt{\rho}}\right)\rho\mathrm{d}\rho + \frac{W_\nu}{V_0 S}. \end{aligned} \tag{6.8}$$

The total mass M of the liquid can be subdivided into three volumes contained, respectively, in the column of length L_1, in the channel of length L, and in the cavity of length L_2. In each volume, the liquid has a different velocity due to the different cross-sections. Considering this aspect, an equivalent mass M' is considered:

$$M' = M\left(1 + \frac{L_1}{L}\frac{s}{S_1} + \frac{L_2}{L}\frac{s}{S_2}\right). \tag{6.9}$$

With a unique velocity, the momentum of which is equal to that of the three volumes together, the applied mechanical power is deduced from Eq. (6.8) after the viscous dissipation W_ν has been determined.

The viscous losses result from the friction between different layers of the liquid in the full volume of the channel. The viscosity in the central tube and in the cavity will be neglected due to the very small velocity value in these two volumes. In the following, it is considered that this viscous loss is effective only in a thin layer near the wall of the channel, which agrees with the suggestion that cap R_ω is a hypothesis $R_\omega \gg 1$, Eq. (4.11). Therefore, the viscous loss is evaluated in terms of the distance from the wall, by using for integration the variable $\xi = e(r)/2 - z$ instead of z, Eq. (4.5). Under these conditions the viscous loss is

$$\begin{aligned} W_{\text{visc}} = & -2\int\limits_{volume}\frac{\mathrm{d}\tau}{\mathrm{d}\xi}V\mathrm{d}v \\ = & -2\int\limits_{\infty}^{1}\int\limits_{r_0}^{r}\left(V_0^2\left(\mu'\left(i\frac{\omega}{\nu}\right)\mathrm{e}^{-\sqrt{i\omega/\nu}\xi} - \mu'\left(i\frac{\omega}{\nu}\right)\mathrm{e}^{-2\sqrt{\omega/\nu}\xi}\right)2\pi r dr\right)\mathrm{d}\xi, \end{aligned} \tag{6.10}$$

where V is the local velocity at a distance ξ from the wall, $\tau = -\mu'\mathrm{d}V/\mathrm{d}\xi$ is the local viscous force per unit of surface at a distance ξ from the wall, and μ is the dynamic viscosity of the liquid. The coefficient 2 is due to the fact that there are two boundary layers in the channel. Finally, the viscous loss reads

$$\overline{W}_\nu = \Re\mathrm{e}\left\{\int\limits_{V_0 l} -d\tau\frac{d\xi}{V}\mathrm{d}v = \pi\frac{R^2 - r_0^2}{r_0}V_0^2\mu^*\frac{1+i}{\sqrt{2}}\sqrt{R_\omega}\right\}, \tag{6.11}$$

where $\overline{W}_\nu$ is the effective value over the time of the pulsating power loss. By introducing Eq. (6.11) into the expression for pressure, finally we derive

$$\begin{aligned} P_1' = & \frac{\mathrm{Rm}}{\mathrm{Rm}^*}\left(-i\frac{\gamma P_0 r_0 s}{V_C} + \frac{i\mathrm{Rm}^{*2}M'}{s(\mu\sigma)^2 r_0^3}\right) \\ & + \frac{B_0^2}{\mu\sqrt{2\pi\mathrm{Rm}^*}}\mathrm{e}^{-i\frac{\pi}{8}}\gamma_1\int\limits_{\sqrt{\mathrm{Rm}^*}}^{\sqrt{\mathrm{Rm}^*}Rr_0^{-1}}\frac{\partial}{\partial\rho}\left(\frac{\mathrm{e}^{\rho\mathrm{e}^{i\pi/4}}}{\sqrt{\rho}}\right)\rho\mathrm{d}\rho \\ & + \frac{1}{4e_0}(1+i)\mu'\sqrt{2R_\omega}\frac{\mathrm{Rm}}{\mu\sigma r_0}\left[\left(\frac{R}{r_0}\right)^2 - 1\right]. \end{aligned} \tag{6.12}$$

7. Performances of the generator.

In this section, the performance of the generator is determined by fixing the required electrical power and calculating the needed mechanical power.

7.1. Electrical power. The electrical power is expressed by Eqs. (5.5) and (5.6) in terms of the current I in the load:

$$W_{\mathrm{e}} = \frac{R|\mathbf{I}|^2}{2}. \tag{7.1}$$

The following expressions are derived for vertical and horizontal coils, respectively:

$$W_{\mathrm{e}} = \frac{1}{2} N^2 B_0^2 R \left| \frac{-i \mathrm{e}^{-i\frac{\pi}{8}} \frac{\gamma_1 e_0 \sqrt{2\pi}}{\mu} \int\limits_{\sqrt{\mathrm{Rm}^*}}^{\sqrt{\mathrm{Rm}^*} R/r_0} \sqrt{\rho} \mathrm{e}^{\rho \mathrm{e}^{i\pi/4}} \mathrm{d}\rho + \frac{2\mathrm{Rm}\pi e_0}{\mu} \left(\frac{R^2}{r_0^2} - 1 \right) 2}{\sigma e_0 R} \right|^2 \tag{7.2}$$

and

$$W_{\mathrm{e}} = \frac{1}{2} N^2 B_0^2 R \frac{e_0 \sqrt{2\pi}}{\left(\frac{R}{r_0} - 1 \right) \mu} \times \left| \frac{-i \mathrm{e}^{-i\frac{\pi}{8}} \frac{\gamma_1}{r_0} \int\limits_{r_0}^{R} \int\limits_{\sqrt{\mathrm{Rm}^*}}^{\sqrt{\mathrm{Rm}^*} r/r_0} \frac{\mathrm{e}^{-i\frac{\pi}{8} + \rho \mathrm{e}^{i\pi/4}}}{\sqrt{\rho}} \rho \mathrm{d} + \frac{2\mathrm{Rm}\pi e_0}{\mu} \left(\frac{R^2}{r_0^2} - 1 \right) 2}{\sigma e_0 R} \right| \tag{7.3}$$

7.2. Mechanical power. The mechanical power corresponds to the efficient value over one period of the scalar product of the pressure applied by the resulting velocity to the free surface of the central duct. The velocity is assumed to be the origin of the phases.

$$W_{\mathrm{mech}} = \frac{1}{2} \overline{p_1' S V}. \tag{7.4}$$

Considering the flowrate continuity as

$$S_1 V_1 = S V, \tag{7.5}$$

where S_1 and V_1 are, respectively, the cross-section of the central duct and the free surface velocity, and S, V are the cross-section of the channel and the velocity of the conducting fluid inside at a generic point of the channel, it is found that Eq. (7.4) holds valid at any point of the channel. The resulting expression for the mechanical power reads

$$W_{\mathrm{mech}} = \frac{1}{2} \frac{\mathrm{Rm} \cdot s}{\mu \sigma r_0} \Re\mathrm{e} \left\{ \frac{B_0^2}{\mu \sqrt{\mathrm{Rm}^*}} \mathrm{e}^{-i\frac{\pi}{8}} \gamma_1 \int\limits_{\sqrt{\mathrm{Rm}^*}}^{\sqrt{\mathrm{Rm}^*} R/r_0} \frac{\partial}{\partial \rho} \left(\frac{\mathrm{e}^{\rho\, \mathrm{e}^{i\theta}}}{\sqrt{2\pi\rho}} \right) \rho \, \mathrm{d}\rho \right. + \left. \frac{1}{4e_0} (1+i) \mu' \sqrt{2R_\omega} \frac{\mathrm{Rm}}{\mu \sigma r_0} \left[\left(\frac{R}{r_0} \right)^2 - 1 \right] \right\}. \tag{7.6}$$

Eq. (7.5) is the same for both vertical and horizontal coils; the differences result from the different values of γ_1. The ratio between electrical and mechanical energies provides the efficiency of the engine.

Table 1. Main parameters and possible performances of the system.

Channel internal radius r_0, [mm]	40
Channel inlet height e_0, [mm]	3
Channel external radius R, [mm]	160
Applied induction field B_0, [T]	0.3
Fluid conductivity σ, [S]	10^7
Fluid magnetic permeability μ, [H/m]	$4\pi \cdot 10^{-7}$
Number of turns of the coil N	280
Cavity volume V_c, [m^3]	$3{\cdot}10^{-2}$
Equivalent mass of liquid, [kg]	0.25
Channel cross-section, [m^2]	10.05
Magnetic Reynolds number Rm	3
Skin effect parameter Rm*	0–1500
Max electric power (vertical coil) W_e^{max}, [W]	300
Max electric power (horizontal coil) W_e^{max}, [W]	1200
Max mechanical power (vertical coil) W_m^{max}, [W]	600
Max mechanical power (horizontal coil) W_m^{max}, [W]	10 000
Max efficiency (vertical coil) η^{max}, %	50
Max efficiency (horizontal coil)η^{max}, %	14
Limited amplitude of pressure P_1, [bar]	5

8. Main results.

The main results that concern the comparison between the two systems are given in terms of performance, and they are presented in the form of a 3D diagram for mechanical and electrical power as well as for pressure evolution and efficiency. The influence of viscosity in terms of losses is also expressed by the velocity distribution inside the boundary layer. The results are given for the imposed pressure 50 bar.

The following results have been obtained under the values summarized in Table 1.

The first 3D diagrams compare the electricity production against the frequency, which is represented by $\mathrm{Rm}^* = \omega r_0^2 \mu_0 \sigma$.

The electrical power (see Figs. 3*a*,*b*) makes obvious that the power produced by the horizontal coil is much higher compared to the vertical one. However, as will be shown below, the mechanical power needed to obtain this power is much higher for the horizontal coil than for the vertical coil.

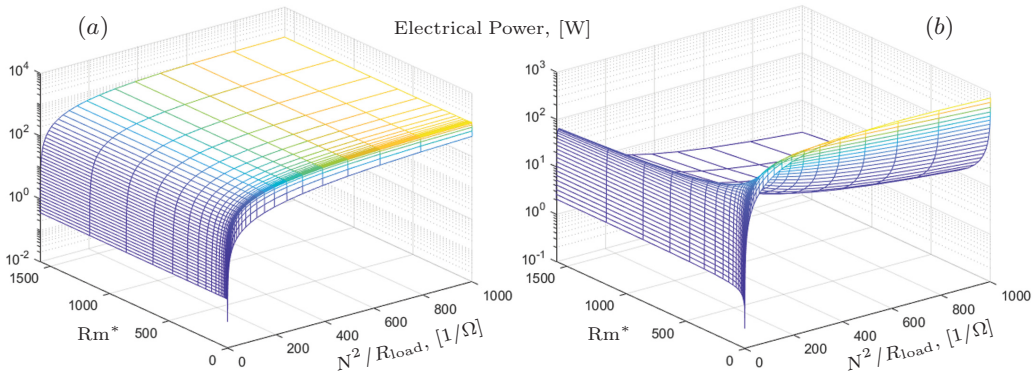

Fig. 3. Electrical power for (*a*) the horizontal coil and (*b*) vertical coil.

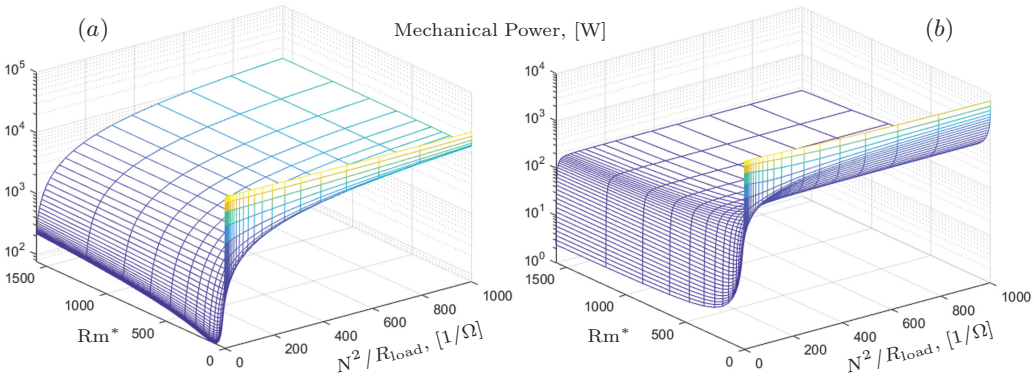

Fig. 4. Mechanical power for (*a*) the horizontal coil and (*b*) vertical coil.

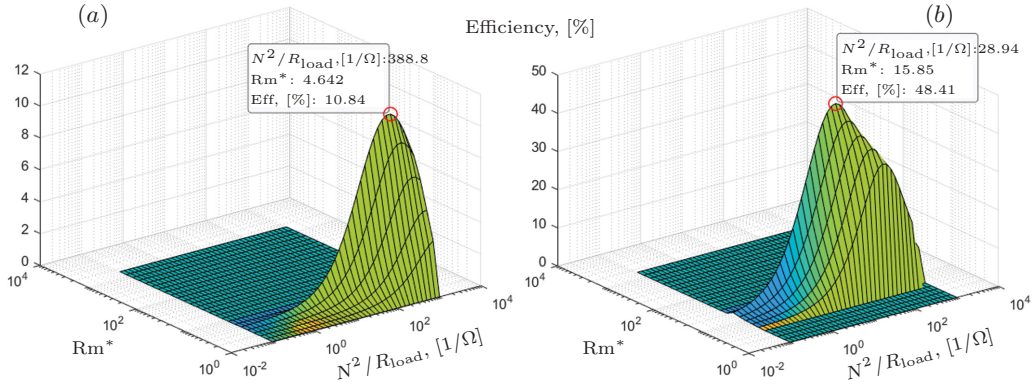

Fig. 5. Efficiency for (*a*) the horizontal coil and (*b*) vertical coil with a limited value of oscillating pressure at 5 bars.

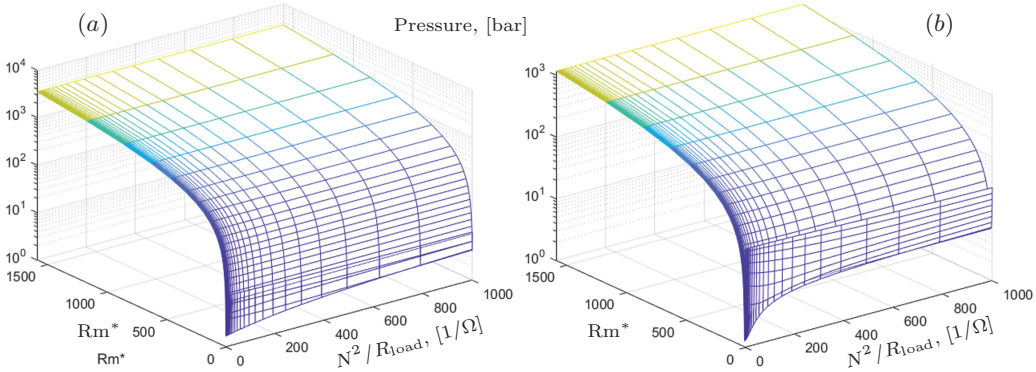

Fig. 6. Pressure for (*a*) the horizontal coil and (*b*) vertical coil.

Figs. 4*a*,*b* illustrate the evolution of the mechanical power for the two configurations. The mean value of the 50 bar pressure is assumed. This value is assumed to be compatible with a thermoacoustic device that supplies the electrical generator with the alternate pressure. As anticipated, mechanical power is much more important for the horizontal coil than for the vertical one.

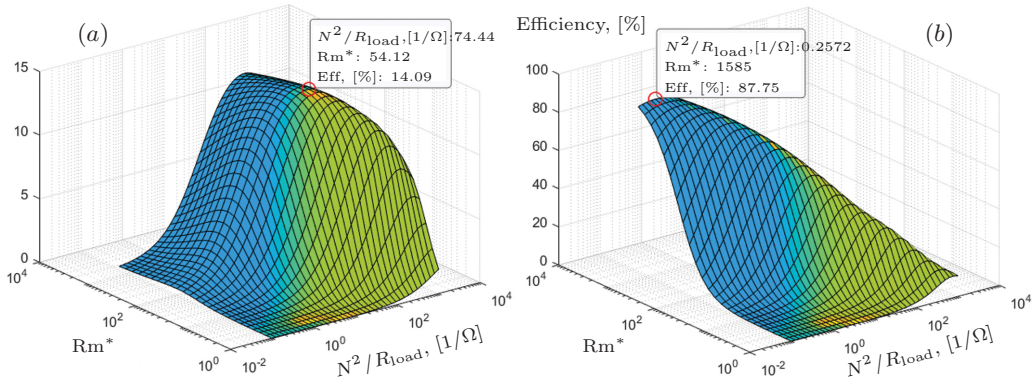

Fig. 7. Efficiency without pressure limitation for (*a*) the horizontal coil and (*b*) vertical coil.

The efficiencies for both configurations (Figs. 5*a*,*b*) are plotted under the restriction to limiting the amplitude of the applied alternate pressure to 10% of the averaged one (50 bar). As expected, the layout with the vertical coil guarantees a much higher efficiency.

The pressure applied needed to obtain a prefixed electrical power (Figs. 6*a*,*b*), with all other things being equal, is much higher for horizontal coils than for vertical ones, where the difference can be attributed to the phase shift between velocity and pressure. The value of the oscillating pressure arises mainly from the electromagnetic forces and induced current in the liquid metal. One way to decrease the pressure level while maintaining constant electrical power is the phase shifting the load using a capacitance.

Suppressing the limitation of pressure, the efficiency (Figs. 7*a*,*b*) can reach an excel-

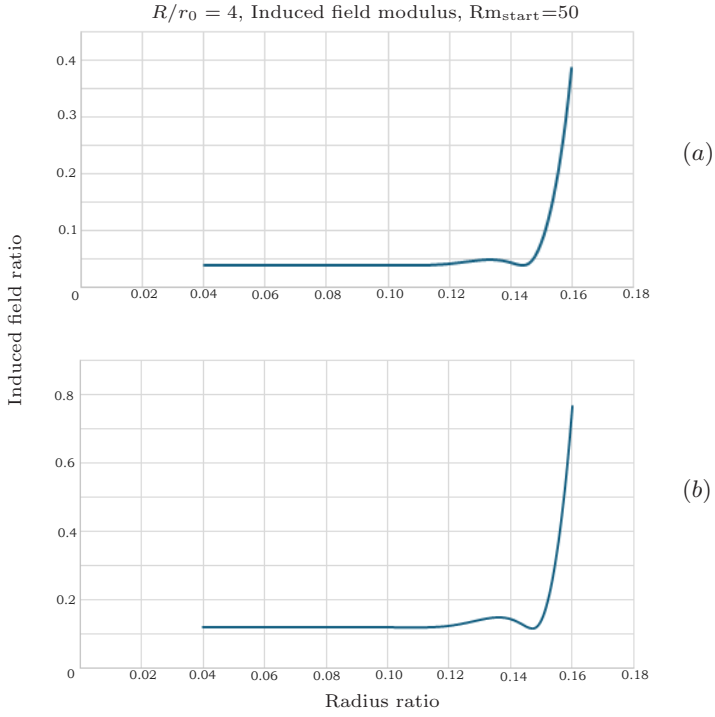

Fig. 8. Dimensionless induced field distribution along the radius for (*a*) the horizontal coil and (*b*) vertical coil.

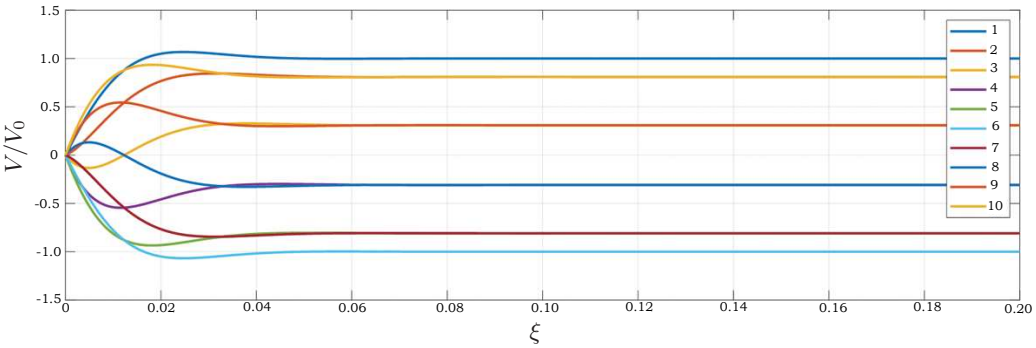

Fig. 9. Velocity distribution along the radius to the wall (ξ) at different time instants during one cycle. In the legend, instant time corresponding to each curve is given by the number in the legend multiplied by $2\pi/\omega$.

lent value for the vertical coil, whereas it is limited for the horizontal coil. However, the corresponding level of pressure necessary to obtain such a high value is not realistic. The only way to obtain such a high value of efficiency is to reduce the phase shift between pressure and velocity.

The graph of the dimensionless induced field along the radius for both configurations is displayed in Figs. 8*a*,*b*. As seen, the induced field seems to be lower for the horizontal coil compared with the vertical one. This can be explained by the fact that the horizontal coil is parallel to the MHD channel, and hence the magnetic field due to the coil tends to decrease continuously due to the induced current (Lentz law). This also explains why the efficiency of the horizontal coil is much lower than that of the vertical one.

As to the velocity profiles, they are given under the assumption that the influence of viscosity is limited to a small depth near the walls of the channel so that the bulk of the flow has a constant value.

Fig. 9 illustrates the distribution of the velocity perpendicularly to the channel wall. As seen, the viscosity introduces a phase shift in the velocity profiles, such as at certain periods of time there arises a counter flow opposite to the bulk flow. This is a classical result in oscillating flows.

The flow disturbance generated by the viscosity is described by Eq. (4.11). As seen, Eq. (8.1) corresponds to a damping wave, but only the first oscillation can be observed because of the high level of damping:

$$\frac{V}{V_0} = \left[\cos(\omega t) - \frac{\cos\left(\omega t - \sqrt{\frac{R_\omega}{2}}\frac{\xi}{r_0}\right)}{\mathrm{e}^{\sqrt{\frac{R_\omega}{2}}\frac{\xi}{r_0}}}\right]. \tag{8.1}$$

The viscous losses can be deduced from the velocity in the boundary layer (Eqs. 6.10, 6.11) with the expression recalled below.

$$\overline{W_\nu} = \frac{\sqrt{2}}{4}\pi\frac{R^2 - r_0^2}{r_0}\frac{\mathrm{Rm}^2}{(\mu\sigma)^2}\mu^*\sqrt{R_\omega}. \tag{8.2}$$

The 3D view of the viscous losses is shown in Fig. 10. These losses are integrated in the efficiency distribution, (Figs. 5*a*,*b*, 7*a*,*b*).

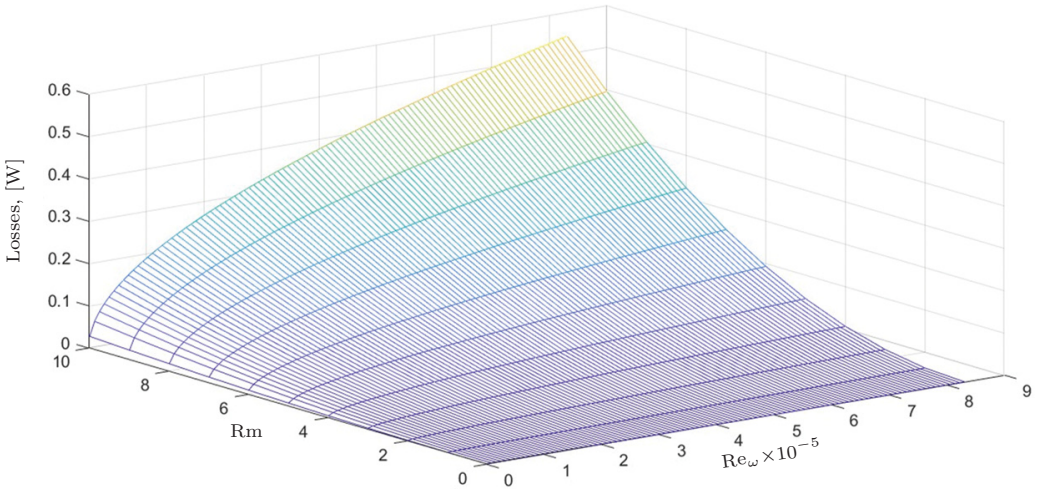

Fig. 10. Power dissipation by viscosity.

In most parts of the considered configurations and, in particular, at $\mathrm{Rm} = 3$, the losses due to viscosity are lower than 50 W.

9. Concluding remarks.

The study discussed in this article relates to the production of electrical energy, taking advantage of an oscillating motion of an electrically conducting liquid in the presence of an imposed magnetic field. Such field can be induced, for example, by permanent magnets, whereas the alternate motion of the liquid can be driven by applying an oscillating pressure, taking advantage of a thermoacoustic engine, which makes it possible to realize a chain that transforms thermal energy into electricity without solid moving parts.

The electric generator leverages magnetic induction to generate an electrical current in the liquid and also to transfer the electrical power to the load, thus avoiding the use of electrodes.

This work compares two coil geometries and considers viscosity minding two aspects: the modified velocity distribution in the boundary layer and the energy dissipation associated.

As to the scale laws, it can be noted that for a fixed geometry, both electrical and mechanical power vary like B_0^2 and Rm^2.

Increasing the depth of the channel also increases both mechanical and electrical energy proportionally.

Maximum efficiency depends on several parameters, such as the geometry of the generator, r_0, $e_0 R$, etc., and the expected electrical power. This work needs to be done for any specific situation. It can be expected that the efficiency of such an electrical generator can reach 0.8 with vertical coils, which is better than with horizontal coils.

Acknowledgements. The work is supported by the Recovery and Resilience Facility project "Internal and External Consolidation of the University of Latvia" (No. 5.2.1.1.i.0/2/24/I/CFLA/007) activity No 2.2 "Implementation of Postdoctoral Grants' by implementing Grant project LU-BA-ZG-2024/1-0002. Project name: "Electromagnetic stabilization studies of a liquid metal free surface for applications in thermoacoustically driven magnetohydrodynamic generator".

References

[1] A. Montisci, M. Caredda. A static hybrid renewable energy system for off-grid supply. *Sustainability*, vol. 13 (2021), p. 9744. https://doi.org/10.3390/su13179744

[2] G.W. Swift, S.L. Garrett. Thermoacoustics: A unifying perspective for some engines and refrigerators. *The Journal of the Acoustical Society of America*, vol. 113 (2003), 2379–2381. https://doi.org/10.1121/1.1561492

[3] M. Petrick, K. Lee. Performance characteristics of a liquid metal MHD generator. US Department of Energy, Office of Scientific and Technical Information *Technical Report No. ANL-6870 (1964) 4681999*. https://doi.org/10.2172/4681999

[4] S. Zhu, G. Yu, C. Jiang et al. A novel thermoacoustically-driven liquid metal magnetohydrodynamic generator for future space power applications. *Energy Conversion and Management*, vol. 258 (2022), p. 115503.

[5] S. Zhu, T. Wang, C. Jiang et al. Experimental and numerical study of a liquid metal magnetohydrodynamic generator for thermoacoustic power generation. *Applied Energy*, vol. 348 (2023), p. 121453.

[6] T. Murakami, Y. Nakata, Y. Okuno, H. Yamasak. An analytical study of the plasma conditions and performance of an MHD generator. *Electrical Engineering in Japan*, vol. 144 (2003), 9–15. https://doi.org/10.1002/eej.10196

[7] P.F. Chester, W.T. Norris, Z. Croitoru. Superconducting magnets for MHD generators. *Philosophical Transactions of the Royal Society of London. Series A, Mathematical and Physical Sciences*, vol. 261 (1967), pp. 558–579.

[8] R.A. Perkins. Electrode materials for coal-fired MHD generators. *Final report (1980) No. EPRI-AP-1562. Lockheed Missiles and Space Co., Palo Alto, CA (USA)*. https://doi.org/10.2172/6723439

[9] M. Ishikawa, M. Fujita, Y. Fujita, J. Umoto. Performance of coal-fired MHD generators with large leakage current. *Energy Conversion and Management*, vol. 34 (1993), pp. 607–617. https://doi.org/10.1016/0196-8904(93)90095-R

[10] R.J. Rosa, C.H. Krueger, S. Shioda. Plasmas in MHD power generation. *IEEE Transactions on Plasma Science*, vol. 19 (1991), pp. 1180–1190. https://doi.org/10.1109/27.125040

[11] A. Alemany, A. Krauze, M.A. Radi. Thermo acoustic MHD electrical generator. In: *Energy Procedia, Impact of Integrated Clean Energy on the Future of the Mediterranean Environment*, vol. 6 (2011), pp. 92–100. https://doi.org/10.1016/j.egypro.2011.05.011 .

[12] A. Alemany, S. Carcangiu, R. Forcinetti et al. Feasibility analysis of an MHD inductive generator coupled with a thermoacoustic resonator. *Magnetohydrodynamics*, vol. 51 (2015), pp. 531–542. https://doi.org/10.22364/mhd.51.3.13

[13] A. Alemany, A. Brekis, A. Montisci. A liquid metal alternate MHD disk generator. *Sustainability*, vol. 15 (2023), p. 12619. https://doi.org/10.3390/su151612619

[14] A. Brekis, A. Alemany, O. Alemany, A. Montisci. Space thermoacoustic radioisotopic powers, SpaceTRIPS: The Magnetohydrodynamic Generator. *Sustainability*, vol. 13 (2021), p. 13498. https://doi.org/10.3390/su132313498

[15] *SpaceTRIPS —FP7 [WWW Document], n.d. CORDIS—European Commission*. https://cordis.europa.eu/project/id/312639/reporting/it (accessed 4.18.24).

Received 16.08.2024